Functionalized mesoporous silicas SBA-15 for heterogeneous photocatalysis towards CECs removal from secondary urban wastewater

Bruna Castanheira [a], Larissa Otubo [b], Cristiano L.P. Oliveira [c], Rosa Montes [d], José Benito Quintana [d], Rosario Rodil [d], Sergio Brochsztain [e], Vítor J.P. Vilar [f,**], Antonio Carlos S.C. Teixeira [a,*]

[a] Research Group in Advanced Oxidation Processes (AdOx), Chemical Systems Engineering Center, Department of Chemical Engineering, Escola Politécnica, University of São Paulo, Av. Prof. Luciano Gualberto, tr. 3, 380, São Paulo, SP, Brazil
[b] Nuclear and Energy Research Institute (IPEN), Av. Prof. Lineu Prestes, 2242, 05508-000, São Paulo, SP, Brazil
[c] Institute of Physics, University of São Paulo, Rua do Matão 1371, 05508-090, São Paulo, SP, Brazil
[d] Department of Analytical Chemistry, Nutrition and Food Sciences, Institute of Research on Chemical and Biological Analysis (IAQBUS), Universidade de Santiago de Compostela, Constantino Candeira S/N, 15782, Santiago de Compostela, Spain
[e] Federal University of ABC, Av. dos Estados, 5001, 09210-580, Santo André, SP, Brazil
[f] Laboratory of Separation and Reaction Engineering-Laboratory of Catalysis and Materials (LSRE-LCM), Department of Chemical Engineering, Faculty of Engineering, University of Porto, Rua Dr. Roberto Frias, 4200-465, Porto, Portugal

HIGHLIGHTS

- First study using TiO_2/SBA-15 for CECs oxidation in an annular FluHelik photoreactor.
- Removal of sulfadiazine (SDZ) from pure water and urban waste water (UWW) spiked with SDZ.
- The activity of TiO_2/SBA-15 in UWW was higher than that of standard TiO_2–P25 for SDZ degradation.
- Adsorption and/or photocatalysis were able to remove other 65 CECs detected in the UWW matrix.

ARTICLE INFO

ABSTRACT

The photocatalytic activity of TiO_2 nanoparticles (NPs) supported on mesoporous silica SBA-15 (TiO_2/SBA-15) was evaluated for the photodegradation of sulfadiazine (SDZ), as target contaminant of emerging concern (CEC), using either pure water solutions (PW) or a real secondary urban wastewater (UWW) spiked with SDZ. For this purpose, TiO_2/SBA-15 samples with 10, 20 and 30% TiO_2 (w/w) were prepared by the sol-gel post synthetic method on pre-formed SBA-15, using titanium (IV) isopropoxide as a precursor. The TiO_2/SBA-15 materials were characterized by HRTEM, SAXS and XRD, nitrogen adsorption isotherms and UV–vis diffuse reflectance spectroscopy. TiO_2 NPs were shown to be attached onto the external surface, decorating the SBA-15 particles. The TiO_2/SBA-15 catalysts were active in SDZ photodegradation using the annular FluHelik photoreactor, when irradiated with UVA light. The 30% TiO_2/SBA-15 sample presented the best performance in optimization tests performed using PW, and it was further used for the tests with UWW. The photocatalytic activity of 30% TiO_2/SBA-15 was higher (56% SDZ degradation) than that of standard TiO_2–P25 (32% SDZ degradation) in the removal of SDZ spiked in the UWW ([SDZ] = 2 mg L^{-1}). The photodegradation of SDZ with 30% TiO_2/SBA-15 eached 90% for UWW spiked with a lower SDZ concentration ([SDZ] = 40 μg L^{-1}). Aside of SDZ, a suit of 65 other CECs were also identified in the UWW sample using LC-MS spectrometry. A fast-screening test showed the heterogeneous photocatalytic system was able to remove most of the detected CECs from UWW, by either adsorption and/or photocatalysis.

---

* Corresponding author.
** Corresponding author.
E-mail addresses: vilar@fe.up.pt (V.J.P. Vilar), acscteix@usp.br (A.C.S.C. Teixeira).

1. Introduction

The shortage of good quality water supplies for the world population has become one of the main challenges of the 21st century. In addition to the pollutants commonly found in water, a new class of contaminants has gained increasing attention in recent years. The so-called contaminants of emerging concern (CECs) are synthetic or natural substances found at low concentrations (ng L^{-1} to µg L^{-1}) in water bodies, and which are suspect of causing hazardous effects to the ecosystem and to the human health (Krzeminski et al., 2019; Rivera-Utrilla et al., 2013; Rodriguez-Narvaez et al., 2017). Pharmaceutical products, antibiotics, hormones and pesticides are relevant examples of CECs. CECs are not regularly monitored in the environment, as there is no regulation for their control in most countries. They are usually not eliminated by conventional water treatment methods, and are then disposed into the environment, where they may accumulate in living organisms. Moreover, wastewater reuse for agriculture might lead to the introduction of CECs in the food chain. Urban wastewater treatment plants (WWTPs) are the main sources of CECs released into the environment, which can induce bacterial resistance and cause damage to aquatic ecosystems (Kovalakova et al., 2020; Kümmerer, 2009a, 2009b).

Different methods for advanced wastewater treatment have been considered in attempt to remove CECs from WWTPs, including adsorption, membrane filtration, ozonation and advanced oxidation processes (AOPs) (Krzeminski et al., 2019; Mohammad et al., 2017; Rivera-Utrilla et al., 2013; Rodriguez-Narvaez et al., 2017). Among AOPs, TiO$_2$-based photocatalysis has been acknowledged as a promising alternative for CECs removal (Fagan et al., 2016; Miranda-García et al, 2010, 2014). TiO$_2$ NPs are low-cost, nontoxic, chemically and physically stable. However, commercially available TiO$_2$ (e.g. P-25) poses some drawbacks, such as low surface area and a tendency to agglomerate in aqueous media. Moreover, small TiO$_2$ particles are difficult to recover by filtration or centrifugation, leading to a difficult separation and recycle, thus limiting its application in industrial scale (Dong et al., 2015). To avoid those problems, in this work it was adopted a strategy reported by several authors, namely the immobilization of TiO$_2$ onto mesoporous silica SBA-15 (Acosta-Silva et al., 2011; Araújo et al., 2016; Besançon et al., 2016; Busuioc et al., 2006; Calzada et al., 2019; Conceição et al., 2017; Lachheb et al., 2011; Liou et al., 2018; Liu et al., 2016; López-Muñoz et al., 2005; Mehta et al., 2016; Salameh et al., 2015; Tseng et al., 2012; Van Grieken et al., 2002; Wei et al., 2018; Yang et al., 2006; Yuan et al., 2020). Different techniques have been employed for the functionalization of SBA-15 with TiO$_2$, including incipient wet impregnation (Calzada et al., 2019), microwave assisted technique (Mehta et al., 2016), direct synthesis (Liou et al., 2018) and sol-gel post-synthetic method (Conceição et al., 2017; Yang et al., 2006), which was the technique employed in the present work. In general, TiO$_2$/SBA-15 materials have shown good efficiency for the degradation of CECs such as dyes (Acosta-Silva et al., 2011; Calzada et al., 2019; Tseng et al., 2012) and other industrial organic contaminants (Conceição et al., 2017; Mehta et al., 2016; Yuan et al., 2020).

To our knowledge, however, all those investigations were limited to batch reactors and synthetic solutions of the contaminant, which are hard to scale up to real systems. In this context, a new concept of light-driven scalable reactor, the annular FluHelik reactor (Espíndola et al., 2019; Moreira et al., 2019) (Fig. S1), which consists of a cylindrical stainless steel shell with inlet and outlet pipes located perpendicularly to the fluid flow on opposite sites and tangentially to the reactor tube in horizontal plane. The single and cylindrical UV lamp is located in a concentric inner quartz sleeve. This design leads to a helicoidal flow around the quartz sleeve allowing a more intense macromixing dynamics, as well as homogenous UV fluence (Fig. S1). Furthermore, the design of the FluHelik photoreactor favors the implementation of several reactors in series, promoting their application on an industrial scale (Espíndola and Vilar, 2020). The FluHelik photoreactor has been successfully employed for homogenous photochemical reactions, such as

UVC/H$_2$O$_2$, UVC/O$_3$ and photo-Fenton, targeting the treatment of leachates from sanitary landfills (pre-industrial scale) (Gomes et al., 2018), slaughterhouse wastewater and CECs removal from secondary urban wastewaters (Alfonso-Muniozguren et al., 2021; Gomes et al., 2021; Barbosa et al., 2020; Espíndola et al., 2019; Espíndola et al., 2021). However, the FluHelik reactor has not yet been tested for AOPs involving heterogeneous catalysis.

In the present work, the FluHelik reactor was used to promote heterogeneous photocatalysis, using a functionalized silica consisting of TiO$_2$ nanoparticles (NPs) supported on SBA-15 mesoporous silica. The system was tested for the photodegradation of sulfadiazine (SDZ) selected as a model of CEC. An example of sulfonamide antibiotics, SDZ is predominantly eliminated in its original form; due to its high stability, about 30–90% of the ingested dose is not absorbed by the body. As a weak acid, SDZ has high solubility (77 mg L^{-1}) and water mobility and has been found in water bodies and wastewater (Balakrishnan et al., 2006; García-Galán et al., 2011). In addition to being able to induce bacterial resistance, SDZ can also cause toxic effects and act as an endocrine disruptor in several living organisms and possibly in humans (Baran et al., 2011; Paulus et al., 2019).

The photocatalytic efficiency of TiO$_2$/SBA-15 in the FluHelik photoreactor was optimized for SDZ oxidation using pure water solutions. Furthermore, the TiO$_2$/SBA-15 photocatalysts were also active in the degradation of SDZ spiked in real urban wastewater (UWW), collected after secondary treatment and tested as a real matrix.

Recently, new analytical methods employing high-resolution mass spectrometry combined with liquid chromatography-quadrupole-time of flight mass spectrometer (LC-QTOF) have allowed the screening of a large number of CECs in water bodies at the ng L^{-1} to µg L^{-1} level in a single run (Paíga et al., 2019; Schymanski et al., 2014; Castro et al., 2021; Wilson et al., 2021). Using LC-QTOF, we were able to detect 65 other CECs present in the UWW sample. Remarkably, irradiation of the UWW in the FluHelik reactor with the TiO$_2$/SBA-15 photocatalysts led to a reduction in the concentration of most of these CECs initially present in the UWW.

2. Experimental

2.1. Chemicals

The following reagents were obtained from Sigma-Aldrich: Pluronic P123 (amphiphilic triblock copolymer, average molecular weight 5,800, 97% purity), tetraethyl orthosilicate (TEOS), sulfadiazine (SDZ, 99% purity) and titanium (IV) isopropoxide (TTIP, 97% purity). Hydrochloric acid and isopropanol were purchased from Baker. Standard TiO$_2$ (Aeroxide® P-25; purity ≥99.5%; specific surface area 55 m^2 g^{-1}) was obtained from Evonik. The real wastewater sample was collected after the secondary treatment of an urban wastewater (UWW) from Portugal in October 2019. Its physicochemical characteristics are summarized in Table S1.

2.2. Catalysts synthesis

2.2.1. Synthesis of pristine SBA-15

The pure SBA-15 matrix was synthesized according to the standard procedure (Zhao et al., 1998), as follows: 4.1 g of Pluronic P123 was dissolved in 30 mL of deionized water under stirring at 35 °C, then 120 g of 2 M HCl aqueous solution was added, and the mixture was stirred for 2 h. In the sequence, 8.5 g (41 mmol) of tetraethylorthosilicate (TEOS) was added and the system was maintained at 35 °C for 24 h under constant stirring. Thereafter, the formed gel was transferred to a mini autoclave, which was sealed and subjected to hydrothermal conditions at 100 °C for 24 h. The sample obtained was washed with 2 L of deionized water, and the precipitated solid was filtrated under vacuum, washed once again with 1 L of deionized water and dried under vacuum for 48 h. Finally, the resulting material was subjected to calcination at

500 °C under N_2 atmosphere for 4 h with a heating rate of 10 °C min⁻¹ to decompose the triblock copolymer and obtain the SBA-15.

2.2.2. Functionalization of SBA-15 with titanium dioxide

The titanium dioxide crystals were deposited onto the SBA-15 surface via sol-gel processing according to the procedure described by Yang et al. (2006). For this purpose, SBA-15 (1.0 g) was sonicated in 50 mL of isopropanol. Different amounts of TTIP were then added, in order to produce samples with different TiO_2 contents, as given in Table 1. Deionized water was slowly added to the resulting mixture (TTIP/water with volumetric ratio of 1/10) to guarantee the hydrolysis of the TTIP. The mixture was stirred for 2 h at room temperature, followed by centrifugation and washing with deionized water. The solid product was dried at 80 °C overnight and then calcined in air at 700 °C for 2 h to obtain the $x\%TiO_2/SBA-15$ catalysts, where $x\%$ represents the wt% of titania loading (Table 1).

2.3. Catalysts characterization

The pristine SBA-15 and $TiO_2/SBA-15$ materials were structurally characterized by N_2 physisorption at 77 K using the Nova 2200 Surface Area and Pore Size Analyzer (Quantachrome). The surface areas were obtained by the BET method, pore volumes were calculated at $P/P_0 = 0.97$ and average pore diameters were obtained by the BJH method (desorption branch).

High resolution transmission electron microscopy (HRTEM) images were obtained with a JEOL JEM 2100 microscope operating at 200 kV. Samples for HRTEM were prepared by drop-casting on aqueous suspension of the mesoporous materials over a carbon-coated copper grid, followed by drying under room conditions. Average particle sizes were calculated from the TEM images with the aid of ImageJ software, by averaging over a large number of individual particles (typically 50–250 NPs).

Small angle X-ray scattering measurements (SAXS) were carried out using a Xeuss 2.0 equipment, with a generating source Xenocs with CuKα (λ = 0.15406 nm) radiation. All the samples were scanned under the same conditions in the range 2θ = 0–3°. The hexagonal cell parameter (a_0) was determined according to Equation (1), where d_{100} corresponds to the Bragg's distance reflection at the (100) crystallography plane.

$$a_0 = \frac{2d_{100}}{\sqrt{3}} \tag{1}$$

The TiO_2 nanocrystals present on the $TiO_2/SBA-15$ materials were characterized with wide-angle XRD patterns recorded on a Bruker (D8-Discover) powder X-ray diffractometer using CuKα radiation of wavelength 0.15406 nm (40 KV, 30 mA), LynxEye detector and Ni filter in the 2θ range 10°–100° with a scanning velocity of 0.75° min⁻¹. From the line broadening of the corresponding X-ray diffraction peaks, the TiO_2 crystallite size was estimated using the Scherrer equation (Equation (2)), where L is the average crystallite size in nm, λ is the wavelength of X-ray radiation (CuKα = 0.154056 nm), K is shape factor, taken as 0.9, β is the broadened profile width at half maximum height in radians and θ is the diffracting angle.

$$L = \frac{K\lambda}{\beta cos\theta} \tag{2}$$

2.4. Photocatalytic assays

2.4.1. Apparatus

Experiments were carried out in the annular FluHelik reactor (Espíndola et al., 2019; Moreira et al., 2019) (Fig. S1) consisting of an outer tube made of borosilicate glass (length = 196.0 mm, internal diameter = 65.6 mm; thickness = 1.8 mm) and an inner quartz sleeve (external diameter = 23.0 mm; thickness = 1.0 mm) filled with an UVC lamp. The reactor is equipped with one inlet and one outlet pipes (length = 43.0 mm, internal diameter = 7.0 mm) located perpendicularly to the fluid flow and tangentially to the shell in horizontal plane and at the top in opposite sides with 3.0 mm distance from reactor ends. The lamp employed was a UVA Philips TL 6 W blacklight blue (λ_{max} = 365 nm) providing a photonic flow in the annular reaction zone of 0.62 ± 0.02 W (Webler et al., 2019). The FluHelik photoreactor was connected to a recirculated cylindrical glass vessel thermostatically controlled and magnetically stirred.

2.4.2. Experimental procedure

The photocatalytic activity of the $TiO_2/SBA-15$ samples was evaluated for the photodegradation of SDZ in the annular FluHelik reactor in multiple pass flow mode (batch system). For this purpose, 1.5 L of a SDZ solution in pure water solution (PW) with $[SDZ]_0 = 2$ mg L⁻¹ was stirred for 24 h (25 °C) with 150 mg of the photocatalyst, in the dark, to reach the adsorption equilibrium. The resulting suspension was placed in the recirculation glass vessel of the reactor, which was pumped to the FluHelik photoreactor by means of a gear pump (Ismatec, model BVP-Z) at a flow rate of 75 L h⁻¹. In all the experiments, the temperature set-point of the refrigerated thermostatic bath was adjusted to keep the solution at 25 °C, and the initial pH was adjusted to 7.0 (after spiking with SDZ) using either H_2SO_4 or NaOH solutions (1.0 mol L⁻¹), but was not corrected over time. After switching on the lamp, aliquots of 10 mL of the aqueous suspensions were collected from the recirculation tank and filtered through a 0.45 μm membrane filter to remove the catalyst powder for further HPLC analysis. The SDZ concentration was monitored by reversed-phase HPLC using a VWR Hitachi ELITE LaChrom apparatus. Details of the analytical system are given as Supplementary Information (SI).

Control experiments with non-modified SBA-15 and with standard TiO_2–P25 were also carried out in the same conditions, as well as in the absence of any catalyst. The pseudo-first-order kinetic constants for SDZ concentration decay (k_{SDZ}) in min⁻¹ was calculated by a nonlinear regression method according to Equation (3), where $[SDZ]_t$ and $[SDZ]_0$ are the concentrations of SDZ at time t and $t = 0$, respectively.

$$[SDZ]_t = [SDZ]_0 \times e^{-k_{SDZ}t} \tag{3}$$

The material that demonstrated the best photocatalytic performance in the previous experiments was chosen for the evaluation of the effect of catalyst mass (50, 150, 200, 300, 500 and 600 mg).

Reusability tests were performed for the best catalyst dose during 4 consecutive cycles. At the end of each cycle, the spent catalyst was filtered off and oven-dried for 24 h (50 °C) before being used for the next run with a fresh SDZ solution.

The matrix effect was evaluated using a real UWW (Table S1) spiked with 2 mg L⁻¹ of SDZ. A control experiment was run in the SDZ-spiked UWW using standard TiO_2–P25 as photocatalyst, in similar conditions, but replacing the 500 mg of 30% $TiO_2/SBA-15$ by 150 mg of P-25 (which contains the equivalent TiO_2 dosage).

A new SDZ-spiked UWW sample was prepared, as above, but with a lower concentration of SDZ ($[SDZ] = 40$ μg L⁻¹), and irradiated in the same conditions (with 500 mg of 30% $TiO_2/SBA-15$). In this experiment, only three aliquots (200 mL each) were collected for analysis: (1) before

Table 1
Description of the $TiO_2/SBA-15$ samples prepared.

Sample	Volume TTIP (mL)[a]	Weight % TiO_2	Ti/Si[b]
10% TiO_2/SBA-15	0.37	10%	0.08
20% TiO_2/SBA-15	0.74	20%	0.15
30% TiO_2/SBA-15	1.11	30%	0.23

[a] Added to 1 g of SBA-15 ($d_{TTIP} = 0.96$ g cm⁻³).
[b] Molar ratio.

catalyst addition; (2) after 24 h in the dark (adsorption period); (3) after 180 min irradiation (photodegradation period). SDZ was extracted from the aliquots by solid-phase extraction (SPE). Briefly, the 200 mL aliquots were filtered (0.45 μm polyamide filters) and passed through 500 mg Oasis HLB cartridges (Waters). After washing and drying the cartridge, the analyte was recovered in 10 mL of methanol. Due to the low SDZ concentration, a more accurate detection system was necessary. The methanolic extracts were then analyzed for SDZ content at the Institute of Research on Chemical and Biological Analysis (IAQBUS) of the University of Santiago de Compostela, using a Liquid Chromatography-triple quadrupolote-Tandem Mass Spectrometry (LC-QQQ-MS/MS) system. More details about the instrumental setup are given in the SI file. Besides SDZ, the samples were also screened for further CECs that were originally present in the UWW sample by LC-high-resolution-quadrupole-time of flight mass spectrometer (LC-QTOF) as detailed in the SI. In this way it was possible to preliminarily evaluate, both the adsorption and photocatalytic potential of 30% TiO$_2$/SBA-15 for the removal of other CECs. More experimental details are given in the SI file.

3. Results and discussion

3.1. Characterization of the photocatalytic materials

Wide-angle diffraction patterns of the synthesized catalysts confirm the formation of crystalline TiO$_2$ (Fig. 1A). Pristine SBA-15 shows only a broad peak centered at 2θ = 20°, corresponding to amorphous silica. In the presence of TiO$_2$, new diffraction peaks appear at 2θ = 25.3°, 37.8°, 48.1°, 55.2° and 62.5°, which become more intense with the increase in TiO$_2$ content. The observed diffraction pattern corresponds to the anatase phase of TiO$_2$ (JCPDS card n° 21–1272, space group *I41/amd*). The peaks correspond to (101), (004), (200), (105) and (204) lattice planes of anatase, respectively. Diffraction peaks due to rutile were not observed, evidencing that anatase was the only TiO$_2$ phase formed. The average crystallite sizes *L*, as obtained from the Scherrer equation assuming spherical particles (Equation (2)), range between 6 and 8 nm (Table S2), which favors the photocatalytic activity (Van Grieken et al., 2002).

SAXS patterns of SBA-15 and of the TiO$_2$/SBA-15 catalysts (Fig. 1B) show the typical reflections of 2D-hexagonal mesostructures (space group *p6mm*), showing that the mesoporous framework survived the functionalization procedure. Five well-resolved diffraction peaks can be seen in the 2θ range 0.5–3.0°, which can be indexed as the (100), (110), (200), (210) and (300) reflections. The hexagonal lattice parameter a_0 (which corresponds to the center-to-center pore distance) can be obtained from the d_{100} spacing using Equation 1, and is given in Table S2. A

slight contraction of the silica framework in the TiO$_2$/SBA-15 samples can be observed, which can be attributed to the calcination at 700 °C to form TiO$_2$ particles.

HRTEM images of SBA-15 and TiO$_2$/SBA-15 are shown in Fig. 2 (additional images are given in Fig. S2). Pristine SBA-15 presented the expected hexagonal array of parallel 1D channels (Fig. 2A and B) (Zhao et al., 1998). In contrast, the images of the TiO$_2$/SBA-15 materials (Fig. 2C, E, G) showed TiO$_2$ NPs decorating most of the surface of the SBA-15 particles. The observed surface coating could account for the disappearance of the amorphous silica band (2θ = 20°) in the XRD pattern (Fig. 1A). Some of the NPs appear to be inside the pores, although their precise location cannot be ascertained. Moreover, some parts of the surface were not covered by the NPs, revealing the naked SBA-15 structure underneath. This finding confirms that the SBA-15 matrix resisted the post-synthesis modification with TiO$_2$, which is in agreement with the SAXS measurements (Fig. 1B).

The high magnification HRTEM images of the TiO$_2$/SBA-15 materials (Fig. 2D, F, H) revealed individual TiO$_2$ NPs on the surface. The diameters calculated from the TEM images for the NPs were 8.1 ± 2.2 nm (10% TiO$_2$/SBA-15), 10.5 ± 2.6 nm (20% TiO$_2$/SBA-15) and 7.6 ± 1.6 nm (30% TiO$_2$/SBA-15), which in general agree with the values determined by the Scherrer equation (Table S2). Some of the NPs show clear diffraction patterns, with a *d*-spacing compatible with that calculated from the (101) diffraction peak (Fig. 1A) at 2θ = 25.3° (d_{101} = 3.5 Å).

The TiO$_2$/SBA-15 samples were further characterized by nitrogen adsorption isotherms (Fig. 3A). The corresponding pore size distributions are shown in the insert of Fig. 3A. Textural parameters are given in Table S2. All the materials presented type IV(a) isotherms with H1 hysteresis loop, which are typical of 2D-hexagonal SBA-15 materials (Zhao et al., 1998). The data in Table S2 suggest that the TiO$_2$ NPs were mainly attached to the external surface of the SBA-15 particles, as seen in the TEM images (Fig. 2), since specific surface areas, pore volumes and pore diameters did not decrease substantially in comparison with SBA-15, as would be expected if the NPs were inside the pores. The surface areas and pore volumes actually increased, which is likely due to the extra external area impinged by the presence of the coating NPs. The large surface areas are beneficial for contaminant molecules to access the exposed active sites, thus favoring photocatalytic performance.

The presence of TiO$_2$ in the samples was further detected in the powder diffuse reflectance spectra of the catalysts (Fig. 3B). The spectra show the typical UV absorption band of TiO$_2$, which is not seen in the spectrum of SBA-15. The spectra end at about 415 nm, corresponding to a bandgap energy of 3.0 eV, and are shifted to longer wavelengths compared to the TiO$_2$–P25 spectrum, showing that the absorption of

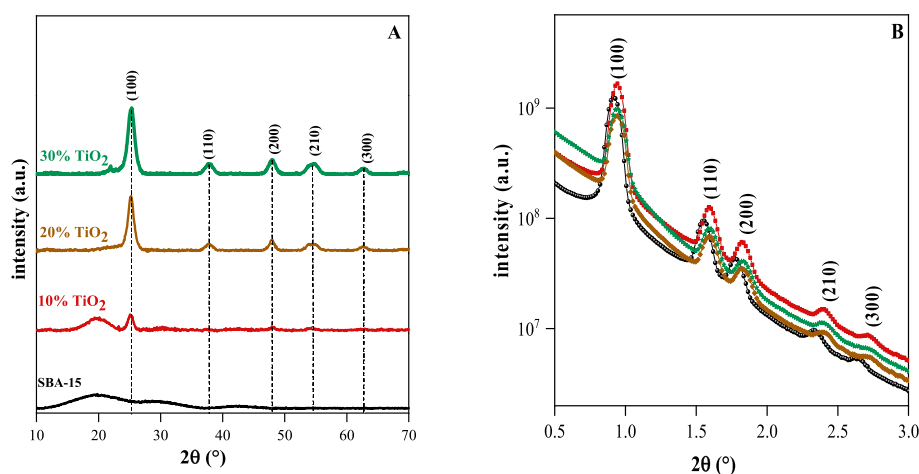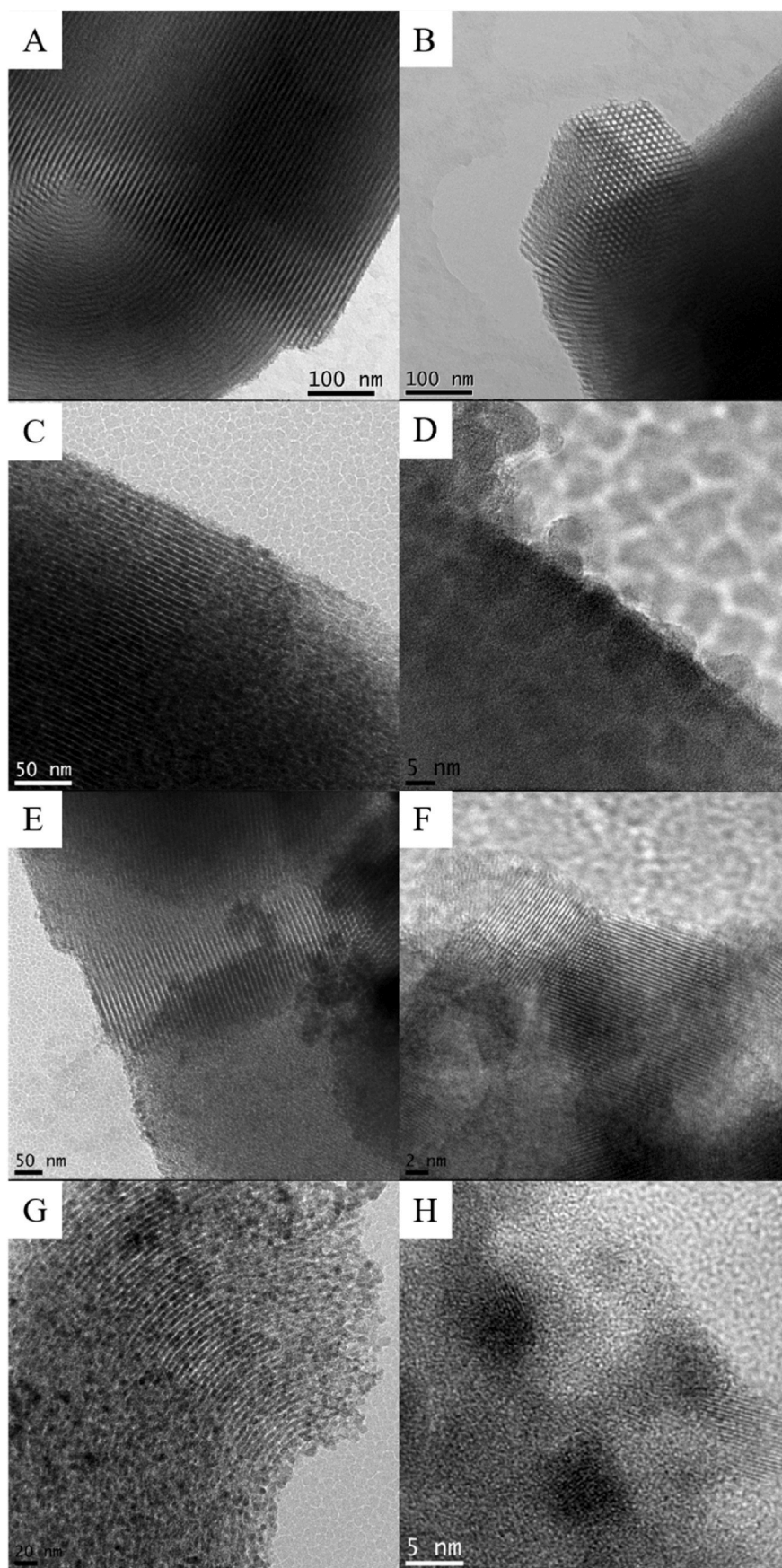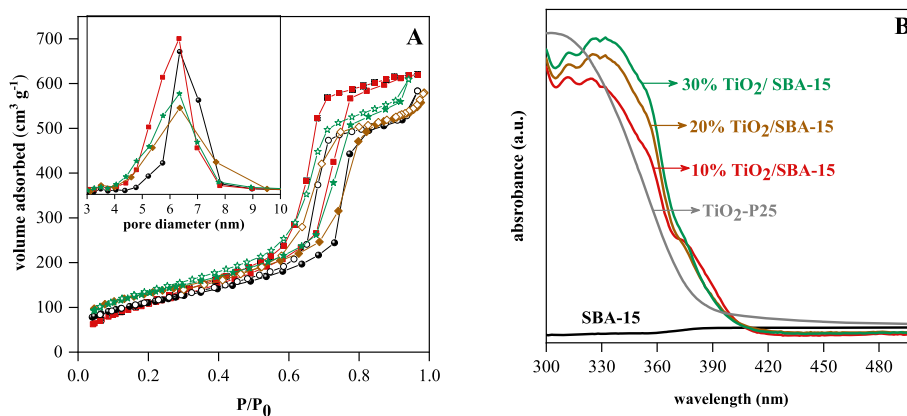**Fig. 1.** (A) Wide-angle XRD patterns of SBA-15 and TiO$_2$/SBA-15 catalysts. (B) Small-angle XRD patterns of SBA-15 (–●–); 10% TiO$_2$/SBA-15 (–■–); 20% TiO$_2$/SBA-15 (–♦–); 30% TiO$_2$/SBA-15 (–★–).

Fig. 2. HRTEM images of pristine SBA-15 (A, B), 10% TiO$_2$/SBA-15 (C, D), 20% TiO$_2$/SBA-15 (E, F) and 30% TiO$_2$/SBA-15 (G, H).

Fig. 3. (A) Nitrogen adsorption isotherms of the TiO$_2$/SBA-15 catalysts. Inset: Pore size distributions (BJH from adsorption branches). Data for pristine SBA-15 are included for comparison. SBA-15 (–●–); 10% TiO$_2$/SBA-15 (–■–); 20% TiO$_2$/SBA-15 (–♦–); 30% TiO$_2$/SBA-15 (–★–). (B) Absorbance spectra (from diffuse reflectance measurements) of the SBA-15, TiO$_2$–P25 and TiO$_2$/SBA-15 catalysts.

UVA radiation by the synthesized TiO2/SBA-15 materials is favored.

3.2. Photocatalytic activity

3.2.1. Effect of TiO$_2$ content on SDZ degradation

The photocatalytic activity of the TiO$_2$/SBA-15 materials was monitored using SDZ as a model CEC. Fig. 4 shows the influence of the TiO$_2$ content on the SDZ degradation kinetics, and the results of the experiments are summarized in Table 2. Note that direct photolysis of SDZ, in homogeneous solution, was almost negligible, reaching only 1.6% of SDZ degradation after 180 min (Table 2). When the non-functionalized SBA-15 was present, ca 14% of the SDZ was removed by adsorption, and only 3% of the SDZ was removed by photo-degradation. In the presence of TiO$_2$, however, most of the SDZ was removed by photocatalysis, rather than adsorption; in fact, only 2–6% of the SDZ was adsorbed on the TiO$_2$/SBA-15 materials. The photocatalytic
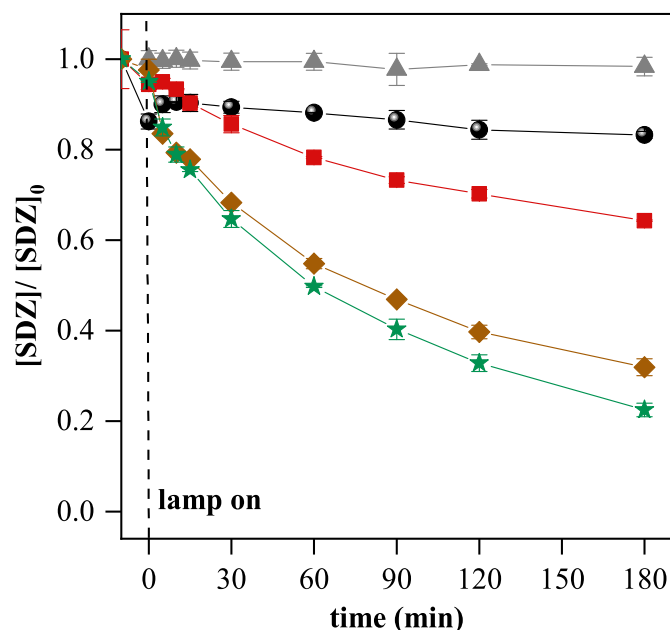
Fig. 4. Photolysis (–▲–), and the photocatalytic performance of SBA-15 (–●–), 10% TiO$_2$/SBA-15 (–■–), 20% TiO$_2$/SBA-15 (–♦–) and 30% TiO$_2$/SBA-15 (–★–) for SDZ photodegradation in the FluHelik photoreactor. Conditions: $m_{photocat}$ = 150 mg; V_{sol} = 1.5 L; [SDZ]$_0$ = 1.88 ± 0.11 mg L^{-1}; pH$_0$ = 7.0; T = 25 °C. Time values below zero represent the adsorption time in the dark (before turning on the lamp) and are out of scale (the actual adsorption time was 24 h).

degradation of SDZ, on the other hand, increased with TiO$_2$ content from 32% (10% TiO$_2$/SBA-15) to 65% (20% TiO$_2$/SBA-15) and to 73% (30% TiO$_2$/SBA-15). Reaction rates also increased with increasing TiO$_2$ content. A four-fold increase in the pseudo-first order kinetic constant was observed as going from 10% to 30% TiO$_2$ (Table 2).

A relevant issue is whether the SDZ is deactivated by the irradiation treatment, forming decomposition products with no capability of inducing bacterial resistance. The photocatalytic degradation of SDZ and other sulfonamides over TiO$_2$ has been studied by several authors (Baran et al., 2009; Batista et al., 2014; Calza et al., 2004; Castanheira et al., 2018; Huang et al., 2015; Liu et al., 2018). The main pathway reported begins with the breakdown of the S–N bond, followed by secondary fragmentation reactions. Baran et al. (2006) and Zessel et al. (2014) have shown that the photolytic products of SDZ degradation were devoid of antibacterial activity, and therefore could not cause bacterial resistance. Moreover, those reports suggest that total mineralization is not necessary for SDZ deactivation. The characterization of the degradation products, however, is out of the scope of the present work.

3.2.2. Effect of the mass of catalyst employed

Considering that 30% TiO$_2$/SBA-15 showed the best photocatalytic performance among the three samples, this material was selected for further experiments. Fig. 5 shows the effect of varying the mass of 30% TiO$_2$/SBA-15 catalyst on SDZ photodegradation. Table 2 shows the corresponding parameters obtained from the experiments. The adsorption of SDZ increased with the increase in the catalyst content, reaching the limiting value of 8% SDZ adsorption. Furthermore, photocatalytic performance was also improved, with the best performance obtained for 500 mg of the 30% TiO$_2$/SBA-15 catalyst, resulting in complete SDZ removal after 120 min of irradiation. A further increase in catalyst mass did not result in a better performance (Fig. 5), both in terms of removal percentage and removal rate, which can be attributed to the increasing turbidity of the suspensions, partially blocking the penetration of the radiation.

3.2.3. Photocatalyst reutilization

From the previous results, the mass of 500 mg of the 30% TiO$_2$/SBA-15 catalyst was selected for the reutilization studies. Fig. 6 shows SDZ photodegradation over three cycles with the selected sample, and Table 2 shows the corresponding parameters. As seen in Table 2, the adsorptive capacity of the material decreased after the first cycle. This result may be an indication that the remaining sulfadiazine, or intermediates formed during photodegradation remain on the surface of the photocatalyst material after the end of the first cycle. The photo-activity, however, remained high in the subsequent cycles, regardless of

Table 2

Percentage of adsorption (% SDZ_{ads}), percentage of photodegradation (% SDZ_{deg}), pseudo-first order reaction rate constant (k_{SDZ}), determination coefficient (R^2) of the nonlinear data fit and initial reaction rate ($r_{0,SDZ}$) values obtained in the degradation experiments of SDZ with TiO_2/SBA-15 catalyst in the FluHelik photoreactor.

Experiment[a]	Matrix[b]	photocatalyst	$m_{photocat}$ (mg)	C_{TiO2} (mg L^{-1})	pH_f	%SDZ ads	%SDZ deg	k_{SDZ} (10^{-2} min^{-1})[c]	R^2
Homogeneous (photolysis)	PW	–	–	–	7.4	–	1.6	–	–
Heterogeneous		**Influence of TiO$_2$ content**							
(photocatalysis)	PW	SBA-15	150	0	7.4	13.8	3.1	0.05	0.97
	PW	10% TiO$_2$/SBA-15	150	15	7.4	5.6	31.6	0.20	0.96
	PW	20% TiO$_2$/SBA-15	150	30	7.2	2.4	65.2	0.61	0.99
	PW	30% TiO$_2$/SBA-15	150	45	7.4	4.9	73.2	0.81	0.99
		Effect of the mass of photocatalyst employed							
	PW	30% TiO$_2$/SBA-15	50	15	7.3	1.4	40.7	0.23	0.98
	PW	30% TiO$_2$/SBA-15	200	60	7.0	6.2	82.5	1.26	0.99
	PW	30% TiO$_2$/SBA-15	300	90	7.1	8.6	87.3	1.86	0.98
	PW	30% TiO$_2$/SBA-15	500	150	7.1	8.4	88.8	2.36	0.99
	PW	30% TiO$_2$/SBA-15	600	180	7.3	8.7	86.2	1.85	0.99
		Photocatalyst reutilization							
	PW	30% TiO$_2$/SBA-15 (1st cycle)	500	150	7.2	9.7	87.3	1.87	0.99
	PW	30% TiO$_2$/SBA-15 (2nd cycle)	500	150	7.1	2.7	94.5	1.72	0.99
	PW	30% TiO$_2$/SBA-15 (3rd cycle)	500	150	7.3	3.1	94.0	1.66	0.99
		Matrix influence							
	PW	TiO$_2$–P25	150	150	6.6	2.2	95.0	6.09	0.99
	UWW	TiO$_2$–P25	150	150	7.2	1.6	31.6	0.25	0.97
	UWW	30% TiO$_2$/SBA-15	500	150	7.6	0.6 (0)[d]	56.4 (90.0)[d]	0.43	0.99

[a] Conditions: V_{sol} = 1.5 L; Irradiation range: 0–180 min; Q = 75 L h^{-1}; [SDZ]$_0$ = 2 mg L^{-1} (nominal value); pH$_0$ = 7.0 (PW), 7.5 (UWW).
[b] PW: Pure water; UWW: Urban wastewater.
[c] Apparent first-order rate constant (k_{app}) of the photocatalytic SDZ degradation.
[d] Data in parenthesis are for the experiment with [SDZ]$_0$ = 40 μg L^{-1} in UWW.
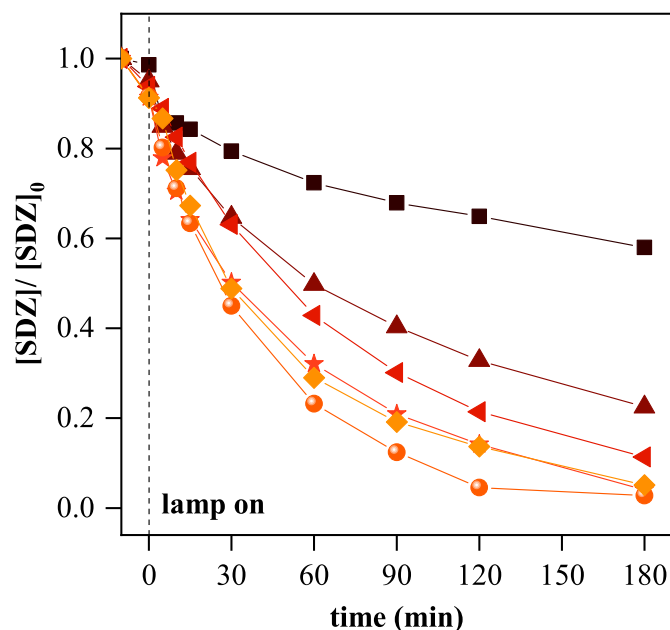
Fig. 5. Photocatalytic performance of 50 mg (—■—), 150 mg (—▲—), 200 mg (—◄—), 300 mg (—★—), 500 mg (—●—) and 600 mg (—◆—) of 30% TiO$_2$/SBA-15 for SDZ photodegradation in the FluHelik photoreactor. Conditions: V_{sol} = 1.5 L; [SDZ]$_0$ = 1.88 ± 0.11 mg L^{-1}; pH$_0$ = 7.0; T = 25 °C. Time values below zero represent the adsorption time in the dark (before turning on the lamp) and are out of scale (the actual adsorption time was 24 h).

the lower adsorption capacity. More than 90% of freshly added SDZ was photodegraded in the second and third cycles, and with nearly the same rate constant as the first cycle (Table 2). The possibility of reutilization is essential for any practical large-scale application.

3.2.4. Performance of TiO$_2$/SBA-15 catalysts in urban wastewater matrix

The degradation of SDZ was also evaluated using a sample of UWW (Table S1), spiked with 2 mg L^{-1} of SDZ. The best condition from the previous experiments, 30% TiO$_2$/SBA-15 (500 mg), was employed here.
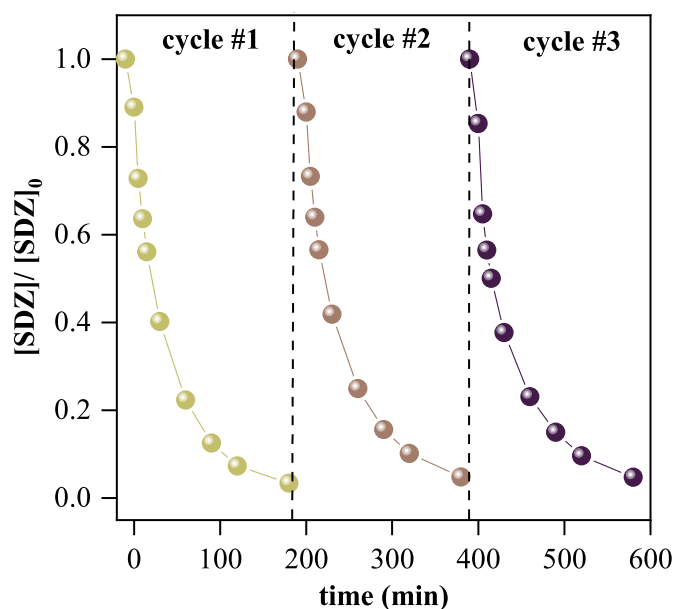
Fig. 6. Reuse of 30% TiO$_2$/SBA-15 for SDZ photodegradation in a FluHelik photoreactor. Conditions: $m_{photocat}$ = 500 mg; V_{sol} = 1.5 L; [SDZ]$_0$ = 1.88 ± 0.11 mg L^{-1}; pH$_0$ = 7.0; T = 25 °C.

The photocatalytic performance of this sample was compared to that of commercially available TiO$_2$–P25. As observed in Fig. 7, TiO$_2$–P25 was more efficient for SDZ degradation than 30% TiO$_2$/SBA-15 in PW. In the UWW, however, the opposite behavior was observed, with TiO$_2$/SBA-15 showing better performance than TiO$_2$–P25.56% SDZ degradation was obtained after 180 min, with 30% TiO$_2$/SBA-15 in the UWW, as compared to 32% SDZ degradation with TiO$_2$–P25 (Table 2). Moreover, SDZ degradation was faster with 30% TiO$_2$/SBA-15, as indicated by the rate constants in Table 2. These results may be due to the reported agglomeration of TiO$_2$–P25 NPs when suspended in wastewater samples, arising from the combined effect of high ionic strength and dissolved organic matter (Romanello and Cortalezzi, 2013; Zhou et al.,
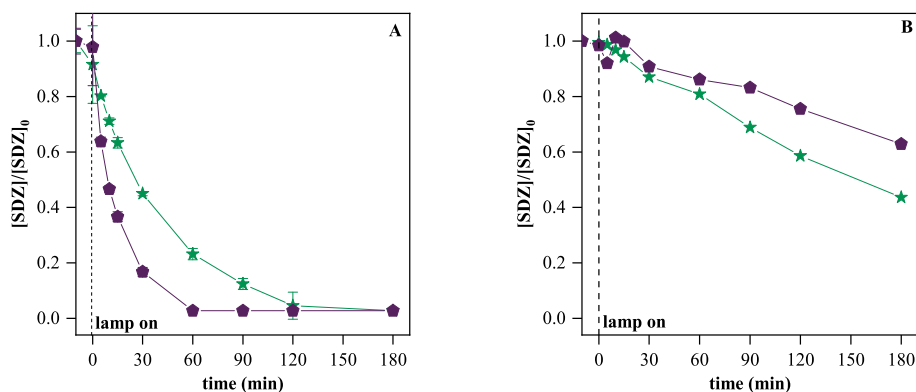
Fig. 7. Comparison between 30% TiO$_2$/SBA-15 (─★─) and TiO$_2$–P25 (─●─) for SDZ photodegradation from (A) PW and (B) UWW matrices in the FluHelik photo-reactor. Conditions: $m_{photocat}$ = 500 mg; V_{sol} = 1.5 L; [SDZ]$_0$ = 1.88 ± 0.11 mg L^{-1}; pH$_0$ = 7.0 (PW) and 7.5 (UWW); T = 25 °C. Time values below zero represent the adsorption time in the dark (before turning on the lamp) and are out of scale (the actual adsorption time was 24 h).

2015; Ren et al., 2017; Xu, 2018). Zhou et al. (2015), for example, showed that TiO$_2$ NPs with 21 nm diameter formed aggregates with sizes greater than 200 nm when dispersed in real wastewater samples. Thus, dispersion of the TiO$_2$ NPs onto the SBA-15 support helped to avoid catalyst nanoparticles agglomeration, leading to a better performance than the standard TiO$_2$–P25 in the real water studied.

The SDZ concentration ([SDZ]$_0$ = 1.88 mg L^{-1}) employed in the optimization experiments reported above is much higher than the [SDZ] expected to be found in real wastewater. Therefore, a new SDZ-spiked UWW sample, with [SDZ] = 40 μg L^{-1}, was prepared and irradiated in the FluHelik, with 500 mg of 30% TiO$_2$/SBA-15 (other conditions as above). For this sample, although the adsorption was null, 90.0% of the

SDZ was removed by photodegradation (Table 2, last entry), stressing the high efficiency of the present system in conditions similar to real conditions.

3.2.5. Removal of other CECs from UWW

The LC-QTOF screening (Castro et al., 2021; Wilson et al., 2021) allowed the detection of 65 other CECs (Table S3), which were originally present in the UWW (not spiked in) (Paíga et al., 2019; Schymanski et al., 2014). The CECs response was then determined in the original UWW (before adding the catalyst), after 24 h in contact with 500 mg of 30% TiO$_2$/SBA-15 and after irradiating the mixture in the FluHelik for 180 min, in the presence of 30% TiO$_2$/SBA-15. The results are displayed
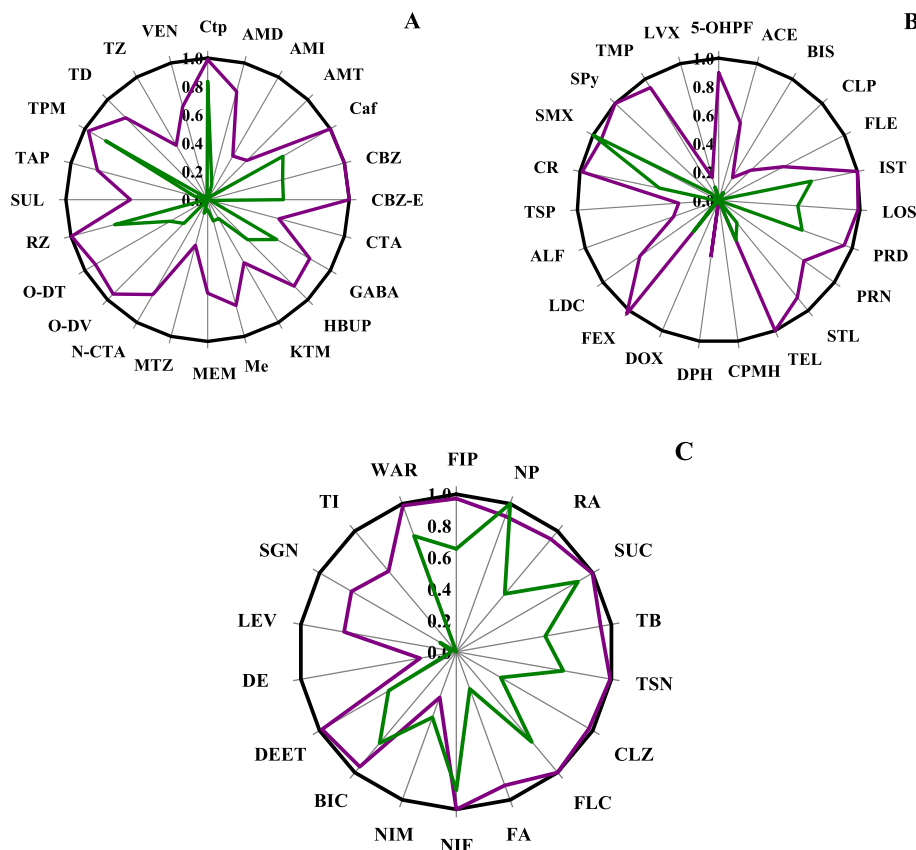

Fig. 8. Radar charts of the response ratios (A/A_0) initially present (──) and after adsorption (──) and photocatalysis in the presence of 30% TiO$_2$/SBA-15 (──), for all detected CECs. (A) Pharmaceuticals for nervous system. (B) Antibiotics and pharmaceuticals for cardiovascular, respiratory and urinary system. (C) Pharmaceuticals for dermatological treatment and other contaminants.

8

in Fig. 8, in the form of radar charts (Paíga et al., 2019), where the contribution of adsorption and photocatalysis for the removal of each drug can be easily visualized, as a percent of the original response (A/A_0). More information is presented in Table S3. With these data, a fast screening can be performed on the activity of TiO$_2$/SBA-15 for the removal of the different CECs, in a single experiment.

In one hand some of the CECs adsorbed strongly onto the catalyst, but were not photodegraded, and on the other hand, other CECs did not adsorb on the catalyst, but were efficiently degraded by photocatalysis (Fig. 8). Since the characterization of the catalyst showed the TiO$_2$ NPs to be located outside the SBA-15 particles, TiO$_2$/SBA-15 presumably acts as a dual-action material for CECs removal, with independent adsorption (mesopores) and photocatalytic (NPs) sites.

The list of CECs found in UWW includes predominantly pharmaceutical drugs used for the neurological system, whose results are displayed in Fig. 8A. It is worth noting that around 70% of neurological drugs were reduced to less than 50% of the original concentration, after adsorption followed by photocatalysis in the FluHelik reactor.

Drugs used as anti-infective and antibacterial agents (Fig. 8B), such as clarithromycin (CR), sulfapyridine (SPy), sulfamethoxazole (SMX), levofloxacin (LVX) and trimethoprim (TMP), did not show adsorption affinity for the surface of the TiO$_2$/SBA-15 catalyst (similarly to SDZ), the same occurring with the cardiovascular drugs losartan (LOS), perindopril (PRD), propranolol (PRN), sotalol (STL), and telmisartan (TEL). However, most of these drugs were efficiently removed after photocatalysis (except for SMX), with nearly complete photodegradation in some cases (SPy, TMP, PRN) (Fig. 8B).

Drugs for dermatological use (Fig. 8C) such as climbazole (CLZ) and fluconazole (II) (FLC), and substances which are not part of the drug class – fipronil (FIP), nitrophenolate (NP), ritalinic acid (RA), sucralose (SUC), terbutrin (TB), and toluene 2-sulfonamide (TSN), were also not adsorbed on the surface of 30% TiO$_2$/SBA-15, and were only partially degraded after photocatalysis. On the other hand, thiemonium (TI), sitagliptin (SGN), levorphanol (LEV), denatonium (DE), and dietiltoluamide (DEET), which are drugs used for other treatments, were completely eliminated after 180 min of irradiation (Fig. 8C).

4. Conclusions

The combination of the FluHelik photoreactor with the TiO$_2$/SBA-15 photocatalyst synthesized in this work was shown to be very promising for the removal of CECs present in UWW. The TiO$_2$/SBA-15 samples were synthesized by the sol-gel post-synthetic method and subsequently characterized by a collection of techniques, such as XRD, SAXS, TEM, nitrogen adsorption-desorption and UV–Vis DRS. Among all candidate catalysts, 30% TiO$_2$/SBA-15 showed the highest catalytic performance under optimal conditions. Moreover, the 30% TiO$_2$/SBA-15 sample was more efficient than standard TiO$_2$–P25 for SDZ degradation in UWW, showing that supporting the TiO$_2$ NPs on SBA-15 effectively inhibited TiO$_2$ agglomeration in this high ionic strength matrix. Furthermore, the FluHelik+30% TiO$_2$/SBA-15 combination was able to remove 90% of the SDZ when spiked at concentrations in the μg L^{-1} range, similar to SDZ concentrations found in the environment. Additionally, tens of other pharmaceutical drugs detected in the UWW sample studied here were also partially or totally removed from the UWW using the FluHelik+30% TiO$_2$/SBA-15 system.

Credit author statements

Bruna Castanheira: Conceptualization, methodology, validation, formal analysis, experimental investigation, data curation, writing – original draft; Larissa Otubo: Formal analysis, data curation, writing – original draft; Cristiano L. P. Oliveira: Formal analysis, data curation, writing – original draft; Rosa Montes: Formal analysis, data curation, writing – original draft; José Benito Quintana: Formal analysis, data curation, writing – original draft; Rosario Rodil: Formal analysis, data curation, writing – original draft; Sergio Brochsztain: Supervision, conceptualization, project administration, writing – original draft; Vítor J. P. Vilar: Supervision, conceptualization, project administration, writing – original draft, resources; Antonio Carlos S. C. Teixeira: Supervision, conceptualization, project administration, writing – original draft, resources, funding acquisition.

Declaration of competing interest

The authors declare that they have no known competing financial interests or personal relationships that could have appeared to influence the work reported in this paper.

Appendix A. Supplementary data

Supplementary data to this article can be found online at https://doi.org/10.1016/j.chemosphere.2021.132023.

References

Acosta-Silva, Y.J., Nava, R., Hernández-Morales, V., Macías-Sánchez, S.A., Gómez-Herrera, M.L., Pawelec, B., 2011. Methylene blue photodegradation over titania-decorated SBA-15. Appl. Catal. B Environ. 110, 108–117. https://doi.org/10.1016/j.apcatb.2011.08.032.

Alfonso-Muniozguren, P., Gomes, A.I., Saroj, D., Vilar, V.J.P., Lee, J., 2021. The role of ozone combined with UVC/H$_2$O$_2$ process for the tertiary treatment of a real slaughterhouse wastewater. J. Environ. Manag. 289, 112480. https://doi.org/10.1016/j.jenvman.2021.112480.

Araújo, M.M., Silva, L.K.R., Sczancoski, J.C., Orlandi, M.O., Longo, E., Santos, A.G.D., Sá, J.L.S., Santos, R.S., Luz, G.E., Cavalcante, L.S., 2016. Anatase TiO$_2$ nanocrystals anchored at inside of SBA-15 mesopores and their optical behavior. Appl. Surf. Sci. 389, 1137–1147. https://doi.org/10.1016/j.apsusc.2016.08.018.

Balakrishnan, V.K., Terry, K.A., Toito, J., 2006. Determination of sulfonamide antibiotics in wastewater: a comparison of solid phase microextraction and solid phase extraction methods. J. Chromatogr. A 1131, 1–10. https://doi.org/10.1016/j.chroma.2006.07.011.

Baran, W., Adamek, E., Sobczak, A., Makowski, A., 2009. Photocatalytic degradation of sulfa drugs with TiO$_2$, Fe salts and TiO$_2$/FeCl$_3$ in aquatic environment-Kinetics and degradation pathway. Appl. Catal. B Environ. 90, 516–525. https://doi.org/10.1016/j.apcatb.2009.04.014.

Baran, W., Adamek, E., Ziemiańska, J., Sobczak, A., 2011. Effects of the presence of sulfonamides in the environment and their influence on human health. J. Hazard. Mater. 196, 1–15. https://doi.org/10.1016/j.jhazmat.2011.08.082.

Baran, W., Sochacka, J., Wardas, W., 2006. Toxicity and biodegradability of sulfonamides and products of their photocatalytic degradation in aqueous solutions. Chemosphere 65, 1295–1299. https://doi.org/10.1016/j.chemosphere.2006.04.040.

Barbosa, I.D., Moreira, F.C., Silva, T.F.C.V., Webler, A.D., Boaventura, R.A.R., Vilar, V.J.P., 2020. Development of a treatment train for the remediation of a hazardous industrial waste land fill leachate: a big challenge. Sci. Total Environ. 741, 140165. https://doi.org/10.1016/j.scitotenv.2020.140165.

Batista, A.P.S., Pires, F.C.C., Teixeira, A.C.S.C., 2014. Photochemical degradation of sulfadiazine, sulfamerazine and sulfamethazine: relevance of concentration and heterocyclic aromatic groups to degradation kinetics. J. Photochem. Photobiol. A Chem. 286, 40–46. https://doi.org/10.1016/j.jphotochem.2014.04.022.

Besançon, M., Michelin, L., Josien, L., Vidal, L., Assaker, K., Bonne, M., Lebeau, B., Blin, J.L., 2016. Influence of the porous texture of SBA-15 mesoporous silica on the anatase formation in TiO2-SiO2 nanocomposites. New J. Chem. 40, 4386–4397. https://doi.org/10.1039/c5nj02859k.

Busuioc, A.M., Meynen, V., Beyers, E., Mertens, M., Cool, P., Bilba, N., Vansant, E.F., 2006. Structural features and photocatalytic behaviour of titania deposited within the pores of SBA-15. Appl. Catal. A Gen. 312, 153–164. https://doi.org/10.1016/j.apcata.2006.06.043.

Calza, P., Medana, C., Pazzi, M., Baiocchi, C., Pelizzetti, E., 2004. Photocatalytic transformations of sulphonamides on titanium dioxide. Appl. Catal. B Environ. 53, 63–69. https://doi.org/10.1016/j.apcatb.2003.09.023.

Calzada, L.A., Castellanos, R., García, L.A., Klimova, T.E., 2019. TiO2, SnO2 and ZnO catalysts supported on mesoporous SBA-15 versus unsupported nanopowders in photocatalytic degradation of methylene blue. Microporous Mesoporous Mater. 285, 247–258. https://doi.org/10.1016/j.micromeso.2019.05.015.

Castanheira, B., Triboni, E.R., Andrade, L.S., Trindade, F.J., Otubo, L., Teixeira, A.C.S.C., Politi, M.J., Queiroz, T.B., Brochsztain, S., 2018. Synthesis of novel periodic mesoporous organosilicas containing 1,4,5,8-naphthalenediimides within the pore walls and their reduction to generate wall-embedded free radicals. Langmuir 34, 8195–8204. https://doi.org/10.1021/acs.langmuir.8b00220.

Castro, V., Quintana, J.B., Carpinteiro, I., Cobas, J., Carro, N., Cela, R., Rodil, R., 2021. Combination of different chromatographic and sampling modes for high-resolution mass spectrometric screening of organic microcontaminants in water. Anal. Bioanal. Chem. https://doi.org/10.1007/s00216-021-03226-6.

Conceição, D.S., Graça, C.A.L., Ferreira, D.P., Ferraria, A.M., Fonseca, I.M., Botelho do Rego, A.M., Teixeira, A.C.S.C., Vieira Ferreira, L.F., 2017. Photochemical insights of TiO2 decorated mesoporous SBA-15 materials and their influence on the photodegradation of organic contaminants. Microporous Mesoporous Mater. 253, 203–214. https://doi.org/10.1016/j.micromeso.2017.07.013.

Dong, H., Zeng, G., Tang, L., Fan, C., Zhang, C., He, X., He, Y., 2015. An overview on limitations of TiO2-based particles for photocatalytic degradation of organic pollutants and the corresponding countermeasures. Water Res. 79, 128–146. https://doi.org/10.1016/j.watres.2015.04.038.

Espíndola, J.C., Cristóvão, R.O., Araújo, S.R.F., Neuparth, T., Santos, M.M., Montes, R., Quintana, J.B., Rodil, R., Boaventura, R.A.R., Vilar, V.J.P., 2019. An innovative photoreactor, FluHelik, to promote UVC/H2O2 photochemical reactions: tertiary treatment of an urban wastewater. Sci. Total Environ. 667, 197–207. https://doi.org/10.1016/j.scitotenv.2019.02.335.

Espíndola, J.C., Vilar, V.J.P., 2020. Innovative light-driven chemical/catalytic reactors towards contaminants of emerging concern mitigation : a review. Chem. Eng. J. 394, 124865. https://doi.org/10.1016/j.cej.2020.124865.

Espíndola, J.C., Caianelo, M., Scaccia, N., Rodrigues-Silva, C., Guimarães, J.R., Vilar, V.J.P., 2021. Trace organic contaminants removal from municipal wastewater using the FluHelik reactor: from laboratory-scale to pre-pilot scale. J. Environ. Chem. Eng. 9, 105060. https://doi.org/10.1016/j.jece.2021.105060.

Fagan, R., Mccormack, D.E., Dionysiou, D.D., Pillai, S.C., 2016. A review of solar and visible light active TiO2 photocatalysis for treating bacteria, cyanotoxins and contaminants of emerging. Concern. Mater. Sci. Semicond. Process. 42, 2–14. https://doi.org/10.1016/j.mssp.2015.07.052.

García-Galán, M.J., Díaz-Cruz, M.S., Barceló, D., 2011. Occurrence of sulfonamide residues along the Ebro river basin Removal in wastewater treatment plants and environmental impact assessment. Environ. Int. 37, 462–473. https://doi.org/10.1016/j.envint.2010.11.011.

Gomes, A.I., Souza-Chaves, B.M., Park, M., Silva, T.F.C.V., Boaventura, R.A.R., Vilar, V.J.P., 2021. How does the pre-treatment of land fill leachate impact the performance of O3 and O3/UVC processes? Chemosphere 278, 130389. https://doi.org/10.1016/j.chemosphere.2021.130389.

Gomes, A.I., Foco, M.L.R., Vieira, E., Cassidy, J., Silva, T.F.C.V., Fonseca, A., Saraiva, I., Boaventura, R.A.R., Vilar, V.J.P., 2018. Multistage treatment technology for leachate from mature urban land fill: full scale operation performance and challenges. Chem. Eng. J. 376, 120573. https://doi.org/10.1016/j.cej.2018.12.033.

Huang, X., Feng, Y., Hu, C., Xiao, X., Yu, D., Zou, X., 2015. Mechanistic QSAR models for interpreting degradation rates of sulfonamides in UV-photocatalysis systems. Chemosphere 138, 183–189. https://doi.org/10.1016/j.chemosphere.2015.05.075.

Kovalakova, P., Cizmas, L., Mcdonald, T.J., Blahoslav, M., Feng, M., Sharma, V.K., 2020. Occurrence and toxicity of antibiotics in the aquatic Environment : a review. Chemosphere 251, 126351. https://doi.org/10.1016/j.chemosphere.2020.126351.

Krzeminski, P., Concetta, M., Karaolia, P., Langenhoff, A., Almeida, C.M.R., Felis, E., Gritten, F., Rasmus, H., Fernandes, T., Manaia, C.M., Rizzo, L., Fatta-kassinos, D., 2019. Performance of secondary wastewater treatment methods for the removal of contaminants of emerging concern implicated in crop uptake and antibiotic resistance spread : a review. Sci. Total Environ. 648, 1052–1081. https://doi.org/10.1016/j.scitotenv.2018.08.130.

Kümmerer, K., 2009a. Antibiotics in the aquatic environment – a review – Part I. Chemosphere 75, 417–434. https://doi.org/10.1016/j.chemosphere.2008.11.086.

Kümmerer, K., 2009b. Antibiotics in the aquatic environment – a review – Part II. Chemosphere 75, 435–441. https://doi.org/10.1016/j.chemosphere.2008.12.006.

Lachheb, H., Ahmed, O., Houas, A., Nogier, J.P., 2011. Photocatalytic activity of TiO2–SBA-15 under UV and visible light. J. Photochem. Photobiol. A Chem. 226, 1–8. https://doi.org/10.1016/j.jphotochem.2011.09.017.

Liou, T.H., Hung, L.W., Liu, C.L., Zhang, T.Y., 2018. Direct synthesis of nano titania on highly-ordered mesoporous SBA-15 framework for enhancing adsorption and photocatalytic activity. J. Porous Mater. 25, 1337–1347. https://doi.org/10.1007/s10934-017-0544-5.

Liu, C., Lin, X., Li, Y., Xu, P., Li, M., Chen, F., 2016. Enhanced photocatalytic performance of mesoporous TiO2 coated SBA-15 nanocomposites fabricated through a novel approach : supercritical deposition aided by liquid-crystal template. Mater. Res. Bull. 75, 25–34. https://doi.org/10.1016/j.materresbull.2015.10.052.

Liu, X., Liu, Y., Lu, S., Guo, W., Xi, B., 2018. Performance and mechanism into TiO2/Zeolite composites for sulfadiazine adsorption and photodegradation. Chem. Eng. J. 350, 131–147. https://doi.org/10.1016/j.cej.2018.05.141.

López-Muñoz, M.J., Grieken, R.V., Aguado, J., Marugán, J., 2005. Role of the support on the activity of silica-supported TiO2 photocatalysts: structure of the TiO2/SBA-15 photocatalysts. Catal. Today 101, 307–314. https://doi.org/10.1016/j.cattod.2005.03.017.

Mehta, A., Mishra, A., Sharma, M., Singh, S., Basu, S., 2016. Effect of silica/titania ratio on enhanced photooxidation of industrial hazardous materials by microwave treated mesoporous SBA-15/TiO2 nanocomposites. J. Nanoparticle Res. 18, 1–9. https://doi.org/10.1007/s11051-016-3523-x.

Miranda-García, N., Maldonado, M.I., Coronado, J.M., Malato, S., 2010. Degradation study of 15 emerging contaminants at low concentration by immobilized TiO2 in a pilot plant. Catal. Today 151, 107–113. https://doi.org/10.1016/j.cattod.2010.02.044.

Miranda-García, N., Suárez, S., Maldonado, M.I., Malato, S., Sánchez, B., 2014. Regeneration approaches for TiO2 immobilized photocatalyst used in the elimination of emerging contaminants in water. Catal. Today 230, 27–34. https://doi.org/10.1016/j.cattod.2013.12.048.

Mohammad, A.B., Zhou, J.L., Ngo, H.H., Guo, W., Thomaidis, N.S., Xu, J., 2017. Progress in the biological and chemical treatment technologies for emerging contaminant removal from wastewater: a critical review. J. Hazard Mater. 323, 274–298. https://doi.org/10.1016/j.jhazmat.2016.04.045.

Moreira, F.C., Bocos, E., Faria, A.G.F., Pereira, J.B.L., Fonte, C.P., Santos, R.J., Carlos, J., Lopes, B., Dias, M.M., Sanromán, M.A., Pazos, M., Boaventura, R.A.R., Vilar, V.J.P., 2019. Selecting the best piping arrangement for scaling-up an annular channel reactor: an experimental and computational fluid dynamics study. Sci. Total Environ. 667, 821–832. https://doi.org/10.1016/j.scitotenv.2019.02.260.

Paíga, P., Correia, M., Fernandes, M.J., Silva, A., Carvalho, M., Vieira, J., Jorge, S., Silva, J.G., Freire, C., Delerue-Matos, C., 2019. Assessment of 83 pharmaceuticals in WWTP influent and effluent samples by UHPLC-MS/MS: hourly variation. Sci. Total Environ. 648, 582–600. https://doi.org/10.1016/j.scitotenv.2018.08.129.

Paulus, G.K., Hornstra, L.M., Alygizakis, N., Slobodnik, J., Thomaidis, N., Medema, G., 2019. The impact of on-site hospital wastewater treatment on the downstream communal wastewater system in terms of antibiotics and antibiotic resistance genes. Int. J. Hyg Environ. Health 222, 635–644. https://doi.org/10.1016/j.ijheh.2019.01.004.

Ren, X., Horn, H., Frimmel, F.H., 2017. Aggregation behavior of TiO2 nanoparticles in municipal effluent: influence of ionic strengthen and organic compounds. Water Res. 123, 678–686. https://doi.org/10.1016/j.watres.2017.07.021.

Rivera-Utrilla, J., Sánchez-Polo, M., Ferro-García, M.Á., Prados-Joya, G., Ocampo-Pérez, R., 2013. Pharmaceuticals as emerging contaminants and their removal from water. A review. Chemosphere 93, 1268–1287. https://doi.org/10.1016/j.chemosphere.2013.07.059.

Rodriguez-Narvaez, O.M., Peralta-Hernandez, J.M., Goonetilleke, A., Bandala, E.R., 2017. Treatment technologies for emerging contaminants in water: a review. Chem. Eng. J. 323, 361–1380. https://doi.org/10.1016/j.cej.2017.04.106.

Romanello, M.B., Cortalezzi, M.M.F., 2013. An experimental study on the aggregation of TiO2 nanoparticles under environmentally relevant conditions. Water Res. 47, 3887–3898. https://doi.org/10.1016/j.watres.2012.11.061.

Salameh, C., Nogier, J.-P., Launay, F., Boutros, M., 2015. Dispersion of colloidal TiO2 nanoparticles on mesoporous materials targeting photocatalysis applications. Catal. Today 257, 35–40. https://doi.org/10.1016/j.cattod.2015.03.025.

Schymanski, E.L., Jeon, J., Gulde, R., Fenner, K., Ruff, M., Singer, H.P., Hollender, J., 2014. Identifying small molecules via high resolution mass spectrometry: communicating confidence. Environ. Sci. Technol. 48, 2097–2098. https://doi.org/10.1021/es5002105.

Tseng, H.H., Lee, W.W., Wei, M.C., Huang, B.S., Hsieh, M.C., Cheng, P.Y., 2012. Synthesis of TiO2/SBA-15 photocatalyst for the azo dye decolorization through the polyol method. Chem. Eng. J. 210, 529–538. https://doi.org/10.1016/j.cej.2012.09.036.

Van Grieken, R., Aguado, J., López-Muoz, M.J., Marugán, J., 2002. Synthesis of size-controlled silica-supported TiO2 photocatalysts. J. Photochem. Photobiol. A Chem. 148, 315–322. https://doi.org/10.1016/S1010-6030(02)00058-8.

Webler, A.D., Moreira, F.C., Dezotti, M.W.C., Mahler, C.F., Barbosa, I.D., Boaventura, R.A.R., Vilar, V.J.P., 2019. Development of an integrated treatment strategy for a leather tannery landfill leachate. Waste Manag. 89, 114–128. https://doi.org/10.1016/j.wasman.2019.03.066.

Wei, J.Q., Chen, X.J., Wang, P.F., Han, Y.B., Xu, J.C., Hong, B., Jin, H.X., Jin, D.F., Peng, X.L., Li, J., Yang, Y.T., Ge, H.L., Wang, X.Q., 2018. High surface area TiO2/SBA-15 nanocomposites : synthesis, microstructure and adsorption-enhanced photocatalysis. Chem. Phys. J. 510, 47–53. https://doi.org/10.1016/j.chemphys.2018.05.012.

Wilson, E.W., Castro, V., Chaves, R., Espinosa, M., Rodil, R., Quintana, J.B., Vieira, M.N., Santos, M.M., 2021. Using zebrafish embryo bioassays combined with high-resolution mass spectrometry screening to assess ecotoxicological water bodies quality status: a case study in Panama rivers. Chemosphere 272, 129823. https://doi.org/10.1016/j.chemosphere.2021.129823.

Xu, F., 2018. Review of analytical studies on TiO$_2$ nanoparticles and particle aggregation, coagulation, flocculation, sedimentation, stabilization. Chemosphere 212, 662–677. https://doi.org/10.1016/j.chemosphere.2018.08.108.

Yang, J., Zhang, J., Zhu, L., Chen, S., Zhang, Y., Tang, Y., Zhu, Y., Li, Y., 2006. Synthesis of nano titania particles embedded in mesoporous SBA-15: characterization and photocatalytic activity. J. Hazard Mater. 137, 952–958. https://doi.org/10.1016/j.jhazmat.2006.03.017.

Yuan, S., Wang, M., Liu, J., Guo, B., 2020. Recent advances of SBA-15-based composites as the heterogeneous catalysts in water decontamination: a mini-review. J. Environ. Manag. 254, 109787. https://doi.org/10.1016/j.jenvman.2019.109787.

Zessel, K., Mohring, S., Hamscher, G., Kietzmann, M., Stahl, J., 2014. Biocompatibility and antibacterial activity of photolytic products of sulfonamides. Chemosphere 100, 167–174. https://doi.org/10.1016/j.chemosphere.2013.11.038.

Zhao, D., Huo, Q., Feng, J., Chmelka, B.F., Stucky, G.D., 1998. Nonionic triblock and star diblock copolymer and oligomeric surfactant syntheses of highly ordered, hydrothermally stable, mesoporous silica structures. J. Am. Chem. Soc. 120, 6024–6036. https://doi.org/10.1021/ja974025i.

Zhou, X.-H., Huang, B.-C., Zhou, T., Liu, Y.-C., Shi, H.-C., 2015. Aggregation behavior of engineered nanoparticles and theis impact on activated sludge in wastewater treatment. Chemosphere 119, 568–576. https://doi.org/10.1016/j.chemosphere.2014.07.037.